ELSEVIER

International Journal of Mass Spectrometry 188 (1999) 155–161

International Journal of Mass Spectrometry

Ion dynamics in a novel linear combined trap

M.A. van Eijkelenborg*, M.E.M. Storkey, D.M. Segal, R.C. Thompson

Blackett Laboratory, Imperial College of Science, Technology and Medicine, Prince Consort Road, London SW7 2BZ, UK

Received 30 November 1998; accepted 25 January 1999

Abstract

We have studied the motional dynamics of ions stored in an ion trap of novel geometry, a linear combined trap, which combines the trapping fields of a linear rf trap and a Penning trap. The motional frequencies of trapped Mg^+ ions are measured as a function of the trapping fields, and we find good agreement with theory. (Int J Mass Spectrom 188 (1999) 155–161) © 1999 Elsevier Science B.V.

Keywords: Laser cooling; Cyclotron resonance; Penning trap; Paul trap

1. Introduction

Linear ion traps have received growing attention in recent years, due to applications in mass spectrometry [1–3], and because linear traps appear to be the most promising way of generating a register of quantum-bits needed for quantum computing [4,5]. It is therefore important to explore the different ways in which a linear trapping environment can be created. We present results obtained using a novel linear trap, the linear combined trap, which can be regarded as a linear Paul trap with a strong magnetic field along the axis. Although it has been indicated that this type of trap can have a number of advantages over existing trap designs [3,6,7], operation of a linear combined trap has not yet been demonstrated experimentally. Some of the spectroscopically important advantages are an increased range of trapping parameters over which stable operation can be obtained, and the possibility to operate the trap with buffer gas cooling [3]. There is in principle no upper mass limit, and compared to the linear Paul trap the lower limit to the mass-to-charge ratio is reduced. Because of the presence of both magnetic and oscillating electric fields the motional dynamics of the ions in the linear combined trap can be quite complicated, but with a proper understanding of the motional frequencies it can be employed as a mass spectrometer for a very large range of masses [1,3].

One can construct different types of linear combined traps with different electrode geometries for the rf fields. A linear combined trap similar to the conventional linear Paul trap would ideally have four parallel rods with hyperbolical cross sections as electrodes [3,8]. Cylindrical rods are conventionally employed, an optimum value of the ratio of rod diameter and rod spacing is used to minimise the consequent deviations from a pure quadrupole. We have, however, chosen to split the ring electrode of a conventional Penning trap into four segments, so that a pure Penning trap results when no rf fields are applied. The

* Corresponding author. E-mail: M.Eijkelenborg@ic.ac.uk

PII S1387-3806(99)00021-4

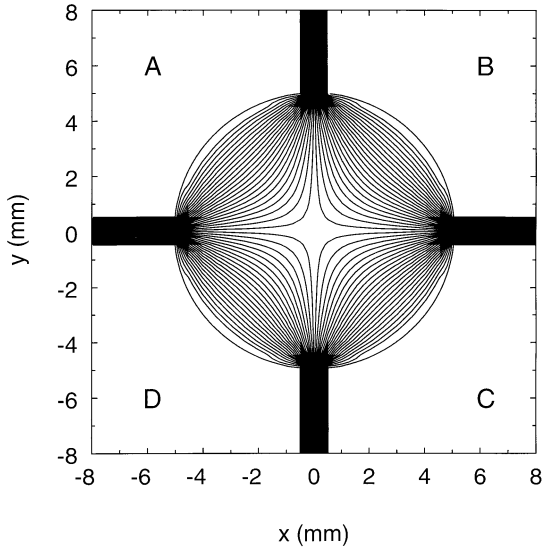

Fig. 1. Split ring electrode of the linear combined trap and the calculated quadrupole equipotential lines. The inner radius R of the ring is 5 mm.

trap is operated with magnesium $^{24}Mg^{+}$ ions which are laser cooled and detected through their fluorescence. The motional frequencies are measured by monitoring the fluorescence level and sweeping the frequency of an external drive applied to one of the trap electrodes [9]. The dependence of the measured frequencies on the various trapping parameters is compared to calculations, and good agreement is found.

2. Split ring linear combined trap

A sideview of the split ring electrode is shown in Fig. 1. A rf field is applied across the four ring segments in order to create a quadrupole near the trap axis. The oscillating voltage on electrodes A and C (see Fig. 1) is in antiphase with the voltage on electrodes B and D. The ring electrode has an inner radius, R, of 5 mm and a thickness of 6 mm. The four copper–beryllium elements of the ring are mounted on a frame using polished ceramic washers of 1 mm thickness and ceramic M2 screws. The resulting near-quadrupole field has been calculated numerically, taking the 1 mm spacing between the split ring electrodes into account, and the resulting equipotential lines are shown in Fig. 1. Despite the "wrong" curvature of the four ring segments in the radial plane and the 1 mm spacing between the electrodes, the potential near the centre of the trap shows only minor deviations from a perfect quadrupole. Rather than using electrode surfaces with a hyperbolic cross section, which are difficult to machine, the trap electrodes have a triangular profile as proposed in [10].

The dc trapping voltage, V_{dc}, was applied to the endcaps which are placed on either side of the ring and have a spacing of 7.1 mm. To compensate for misalignment of the endcaps, a slightly different voltage was applied to each endcap, to ensure that the ion cloud was located in the centre of the ring electrode. In most experiments presented here the voltages were 3.88 V on the one endcap and 4.12 V on the other. In experiments where the dc voltage needed to be varied, we maintained this ratio of endcap voltages, and only quote the average of the two voltages, denoted as V_{dc}. The magnetic field was provided by a conventional electromagnet and the maximum field strength was measured to be 0.99 T. The system was enclosed in an ultrahigh vacuum system kept at a few times 10^{-10} mbar.

The trap was loaded by crossing a beam of Mg atoms with an electron beam at the centre of the trap. The atomic beam oven (containing an isotopic mixture of ^{24}Mg, ^{25}Mg, and ^{26}Mg of natural abundances) is situated just above one endcap electrode while the electron beam emanated from a filament placed behind the other endcap. A hole in the middle of the endcap allowed free passage of the electrons. Our trap loading procedure can lead to trapping of impurity ions (e.g. the ^{25}Mg and ^{26}Mg isotopes or residual gas ions) which are not directly laser cooled. Impurities can slightly shift the centre of mass motional frequencies. No precautions have been taken to prevent this, because its effect on the motional frequencies is small.

The laser radiation required for cooling and detection was generated by intracavity frequency doubling in a Coherent CR699 ring dye laser using an antireflection coated β-barium-borate (BBO) crystal, producing about 150 μW at 280 nm. As an absolute frequency reference we used an iodine absorption cell. The somewhat astigmatic laser beam was sent in

through a 2.5 mm diameter hole between electrodes A and D (see Fig. 1) and was focused to a waist of about 40×80 μm at the centre of the trap. Light scattered by the ions is detected through the hole between electrodes A and B, at right angles to the path of the laser beam. Using a three-lens system the ion cloud was imaged onto a photon-counting photomultiplier. Typically, a cloud of a few hundred ions was loaded into the trap and by repeatedly scanning the laser frequency toward resonance the cloud was cooled. Signal levels were of the order of 100 counts/ms on a background (due to scattered laser light) of 1 count/ms.

3. Cloud temperature

When operated without rf fields, i.e. as a pure Penning trap, the lowest cloud temperatures were obtained. Applying the rf voltage across the ring electrode increases the radial confinement but simultaneously heats the ions due to the induced micromotion. This is illustrated with the measurements shown in Fig. 2, taken with a laser power of 200 μW at 280 nm and $V_{dc} = 4$ V. After optimising the laser beam position the laser frequency is repetitively scanned over 4 GHz for several minutes until a steady state is reached. The laser frequency is scanned at a rate of 1 GHz/s. Every time the laser frequency approaches resonance a strong rise in fluorescence signal is observed. The laser is scanned only slightly over resonance to avoid laser induced heating of the ions. The temperature of the ion cloud, T, is related to the half width at half maximum (HWHM) Doppler width $\Delta\nu$ of the transition through $T = m\lambda^2\Delta\nu^2/2k$ ln 2 (ignoring the contribution from the natural width of the transition). For the case of a pure Penning trap, the ion fluorescence is shown in Fig. 2(a) as a function of laser detuning. Under normal operating conditions a Doppler width of around 100 MHz HWHM is found, which corresponds to a cloud temperature of about 1 K. By using more careful laser beam alignment on a smaller ion cloud the width could be reduced to 40 MHz (the natural linewidth of Mg^+ is 22 MHz). For the linear combined trap, Fig. 2(b), Doppler linewidths of around 700 MHz HWHM are generally

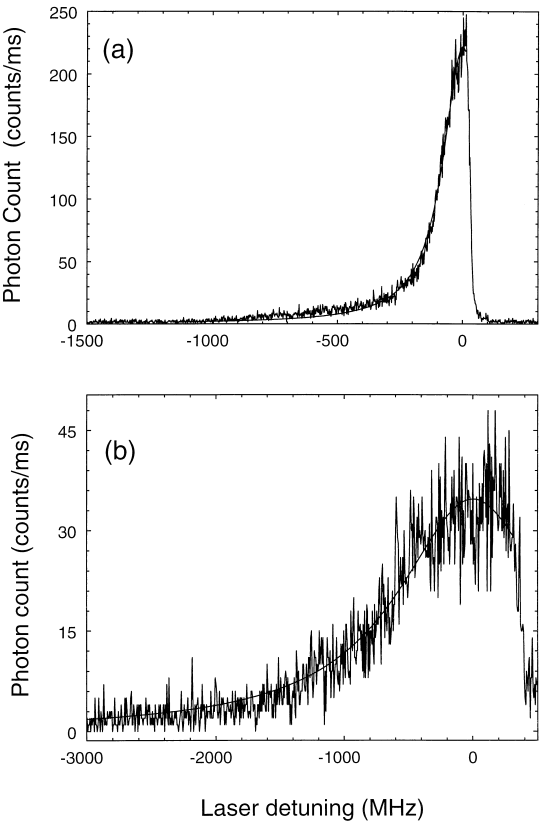

Fig. 2. Laser induced fluorescence of $^{24}Mg^+$ stored in (a) a pure Penning trap, and (b) a linear combined trap when operated at a rf voltage $V_{rf} = 40$ V. From the width of the curves we estimate a cloud temperature of 1 K for the Penning trap (a), and 65 K for the linear combined trap. Note the difference in frequency axes.

found, corresponding to a cloud temperature of 65 K. Generally the cloud temperature in the linear combined trap is higher than in a pure Penning trap as a result of rf heating due to the induced micromotion. The presence of micromotion is corroborated by the observation of strong modulation in the fluorescence photons at the frequency of the rf field [11].

4. Motional frequencies in a linear combined trap

In a linear combined trap the ion's motional frequencies are determined by the magnetic field, the radial confinement due to the rf-quadrupole field, and

the static trapping potential. The three principal motional frequencies are the modified cyclotron frequency, ω_c', the magnetron frequency, ω_m, and the axial frequency, ω_z, which were calculated* by Huang et al. [3]:

$$\omega_c' = \frac{eB}{2m}\left[1 + \sqrt{1 + \frac{4m}{eB^2}\left(\frac{32eV_{rf}^2}{m\pi^2\Omega^2R^4} - \frac{V_{dc}}{a^2}\right)}\right] \quad (1)$$

$$\omega_m = \frac{eB}{2m}\left[1 - \sqrt{1 + \frac{4m}{eB^2}\left(\frac{32eV_{rf}^2}{m\pi^2\Omega^2R^4} - \frac{V_{dc}}{a^2}\right)}\right] \quad (2)$$

$$\omega_z = \sqrt{\frac{2eV_{dc}}{ma^2}} \quad (3)$$

where eB/m is the unmodified cyclotron frequency, V_{rf} is the rf amplitude, $\Omega = 2\pi \times 3.83$ MHz is the rf angular frequency, $R = 5$ mm is the radius of the ring, V_{dc} is the dc trapping voltage, and $a^2 = \pi R^2/2\alpha$ is a geometric factor related to the trap dimensions, with α the trap aspect ratio. From Eq. (3) it is clear that the axial frequency is independent of the rf voltage; it is not affected by a change in the radial confinement (provided that the radial and axial motions are uncoupled, see the following). Note that when the term in parentheses in Eq. (2) becomes zero the magnetron frequency equals zero and the modified cyclotron frequency equals the unmodified cyclotron frequency eB/m. At this value of V_{rf} the radially inward-directed force due to the rf field exactly cancels the radially outward-directed force due to the static electric field on the endcaps.

The ions' motional oscillation frequencies are measured by monitoring their response to an external drive in the form of a small oscillating voltage applied to one or both of the endcaps. For practical reasons the split ring electrode could not be utilised for both the driving and trapping fields simultaneously, even though the radial motions would have been driven more efficiently with such an excitation geometry [13]. The drive signal usually had an amplitude below 10 mV. Since the drive voltage is very small as compared to the voltages applied for trapping, appreciable effects are only expected when the drive is nearly resonant with one of the ions' motional frequencies. At a resonance the ion cloud absorbs energy and changes shape, which can be detected as a change in the level of fluorescence emitted by the cloud when it is irradiated with a laser [9]. The frequency is swept both up and down in frequency across the resonance to eliminate any dependence of the ions response on the direction of the frequency sweep. An example of a frequency sweep is shown in Fig. 3, where the drive frequency is scanned from 150 to 250 kHz and back in 32 seconds. The ion fluorescence shows a clear response at a driving frequency of 200 kHz, both in the forward and backward scan, indicating the axial motional resonance. For all the presented frequency measurements the position at which the change in fluorescence is observed in the forward and backward scan differed by less than 1%. The shape of the

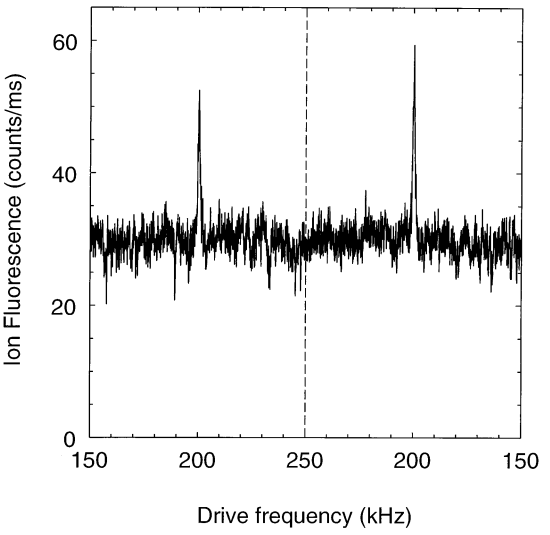

Fig. 3. Change of the observed $^{24}Mg^+$ fluorescence when the drive frequency is swept across the axial motional resonance. The frequency is scanned from 150 to 250 kHz on the left side, and back down from 250 to 150 kHz on the right side of the graph. The trap parameters are $V_{dc} = 5$ V, $V_{rf} = 0$ V, and $B = 0.99$ T.

* The trapping potential near the centre of the trap is slightly stronger in the case of a split ring trap as compared to the four rod trap. Comparing the expressions derived in [3] and [12] we find that the potentials of the two electrode configurations are equal when $r_0^2 = (\pi/8)R^2$, with $2r_0$ the distance between opposing electrode rod surfaces, and R the radius of the split ring electrode.

observed fluorescence change near the resonance is dependent on the laser detuning and alignment, and similar results to those obtained by Imajo *et al.* [9] were found. The small fluctuations in the fluorescence level during the forward scan in Fig. 3 do not reproduce in the backward scan, indicating that they are due to laser power fluctuations. The photon–photon correlation technique that was successfully employed to measure the motional frequencies in a conventional combined trap [14], did not produce any clear frequencies in the case of our linear combined trap.

To determine various trap parameters such as the magnetic field strength B, the aspect ratio α, and a possible contact potential V_{cont}, the motional frequencies of a pure Penning trap ($V_{\mathrm{rf}} = 0$) were measured as a function of the dc trapping voltage V_{dc}. The behaviour of these frequencies is well known [14–16]. From the modified cyclotron frequency we find the (maximum) magnetic field strength, $B = 0.99$ T. The dependence of the axial frequency on V_{dc} provides us with values for the aspect ratio, $\alpha = 1.78(5)$ [which gives $a^2 = 2.20(6) \times 10^{-5}$ m^2], and the contact potential $V_{\mathrm{cont}} = 0.59(9)$ V, which is presumably due to a Mg coating on part of the ring electrode.

We measured the motional frequencies in our linear combined trap both as a function of V_{rf} and as a function of B. First the results obtained as a function of V_{rf} will be discussed. In Fig. 4 the data points indicate the measured frequencies obtained through the changes in fluorescence as shown in Fig. 3. The modified cyclotron, ω_c', the magnetron, ω_m, and the axial, ω_z, motional frequencies are plotted. The solid curves are calculated from Eqs. (1), (2), and (3) using the above determined values of B, α and V_{cont}. The left-most side of Fig. 4 corresponds to a pure Penning trap ($V_{\mathrm{rf}} = 0$). Near the crossover—the point where the magnetron frequency equals zero—we could not obtain data points, since the trap became unstable in the radial direction (see also Sec. 5). Good agreement between theory and experiment is found for all motional frequencies, apart from a slight dependence of the axial frequency on the rf voltage; the frequency decreases from 173 kHz for a pure Penning trap, to 162 kHz at $V_{\mathrm{rf}} = 130$ V. We ascribe this to an

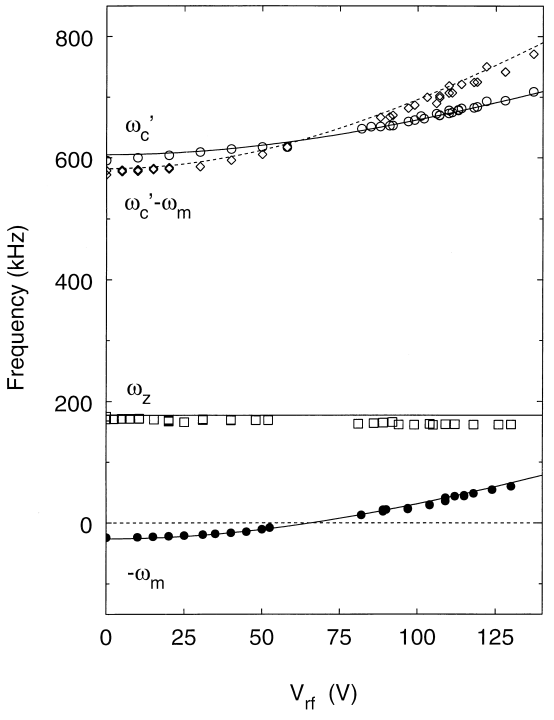

Fig. 4. Motional ion frequencies in a linear combined trap as a function of the rf voltage V_{rf}. The left most side corresponds to a pure Penning trap. The modified cyclotron frequency, ω_c', is indicated by open circles, the magnetron, ω_m, by closed circles and the axial, ω_z, by open squares. We have chosen to plot $-\omega_m$ instead of $+\omega_m$ following the notation in [14,15]. The breathing mode frequencies are indicated by open diamonds.

inaccuracy in the alignment of the trap electrodes; the line through the centres of the endcaps is not quite perpendicular to the plane of the split ring electrode. The design of the trap demands a manual positioning of the endcaps during trap assembly. This procedure is likely to lead to a certain degree of misalignment, causing a coupling of the radial and axial motions. Further coupling can arise because of a misalignment of the endcaps with respect to the magnetic field direction [14]. As a result, the radial confinement created by the rf field causes a slight reduction in the axial confinement, and thereby in the axial frequency. We estimate from the observed frequency shift that the plane of the ring electrode is at a 3° angle with the line through the centre of the endcaps (neglecting possible shifts due to misalignment of the magnetic field).

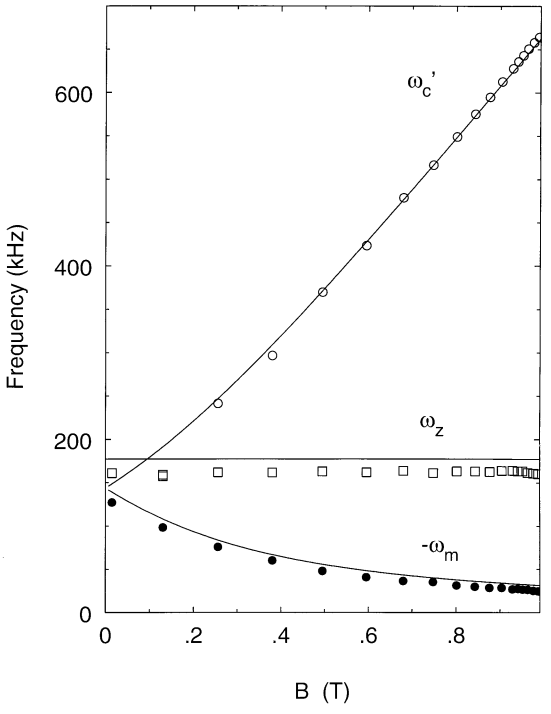

Fig. 5. Motional ion frequencies in a linear combined trap as a function of the magnetic field strength B. The left most side of the graph corresponds to a pure linear Paul trap. The modified cyclotron frequency is indicated by open circles, the magnetron frequency by closed circles and the axial frequency by open squares. We have chosen to plot $-\omega_m$ instead of $+\omega_m$ [14,15].

In addition to the three principal motional frequencies we have also found a strong response at the frequency of the so-called breathing mode (see the open diamonds in Fig. 4), which occurs at $\omega_c' - \omega_m$ [13,17]. These resonance frequencies were obtained as a byproduct during the frequency scan that was designed to reveal the frequency of the modified cyclotron motion, and we ascribe the somewhat larger scatter in these data points to the use of too large a driving voltage.

We have also measured the motional frequencies of the combined trap as a function of B. We determine the value of B by calibrating the voltage across a 1 mΩ shunt resistance placed in the circuit of the electromagnet against a magnetic field probe placed at the position of the trap. In Fig. 5 we present the measured frequencies of the modified cyclotron, the magnetron and the axial motion along with the frequencies calculated from Eqs. (1), (2), and (3). These measurements were performed at a fixed value of V_{rf} = 100 V. We find good agreement between experiment and theory. The axial frequency is again slightly too low, for reasons explained above. The left-most side of Fig. 5 corresponds to a pure linear Paul trap, where one expects only two motional frequencies to appear, the axial and secular frequency ($\omega_m = \omega_c'$). The measured frequencies at low magnetic field strength, however, seem to indicate that the extensive use of this trap in a magnetic field has led to a slight magnetisation of the trap electrodes.

5. Crossover

As was observed in the measurements presented in Fig. 4 the trap becomes unstable near the point where the magnetron frequency becomes zero. This corresponds to the point where the direction of the magnetron motion reverses, changing from co-rotating with respect to the cyclotron motion at low V_{rf} to counter-rotating at high V_{rf}. The value of V_{rf} at which the magnetron frequency is zero is calculated from Eq. (2) and plotted in Fig. 6 (solid curve). The measured data points indicate the largest V_{rf} where a stable signal could still be obtained when increasing V_{rf} from zero. The points all lie below the curve indicating that the ions were lost before the calculated instability point was reached. For practical reasons it was not possible to approach the crossover from the high V_{rf} side. With V_{rf} set to a low value, before the crossover, the laser beam position was set to cool both the modified cyclotron and magnetron motions, i.e. it was given a slight offset in the radial plane [18]. At rf voltages above the crossover the laser beam could be positioned on any part of the cloud, as expected, but best signals were obtained by positioning the laser near the centre of the cloud. As the crossing was approached, the laser beam position had to be given a larger offset in the radial plane, indicating that the centre of the cloud moved away from the geometric centre of the trap. This is due to the presence of contact potentials, which become of crucial impor-

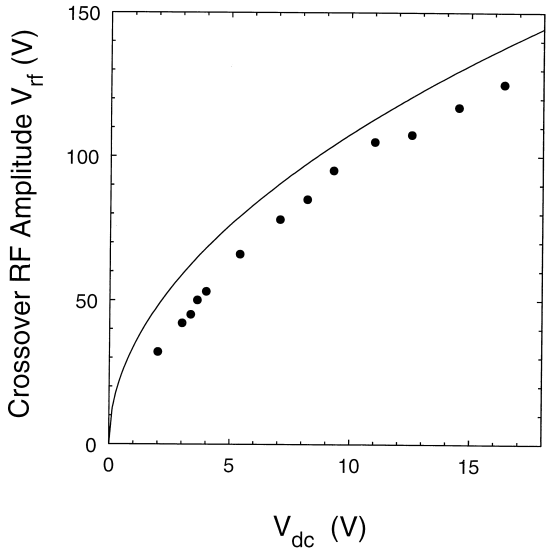

Fig. 6. The data points indicate the maximum rf voltage V_{rf} for which stable trapping signals could still be obtained, plotted as a function of the dc trap potential V_{dc}. The curve is the calculated rf voltage at which the magnetron frequency becomes zero.

tance when the radial confinement becomes very weak. A similar effect was observed and explained in a "normal" combined trap in [14]. This indicates that the suggestion of Huang *et al*. [3] to operate the linear combined trap very close to the crossover point will be very difficult to realise in practice.

6. Conclusions

We have built and operated a linear ion trap of a novel type; the linear combined trap. Being a combination of a Penning trap and linear Paul trap, the resulting ion dynamics is of a complex nature, consisting of a superposition of modified cyclotron, magnetron and axial motions, combined with rf micromotion. We have measured the characteristic motional frequencies of Mg^+ ions stored in a linear combined trap as a function of the two important trapping parameters: the rf amplitude and the magnetic field strength. We find good agreement between theory and experiment. Also we have detected trap alignment imperfections through their effect on the motional frequencies.

Acknowledgements

M.A.v.E. would like to thank the Netherlands Organisation for Scientific Research (NWO) for support. This work was supported by the EP-SRC.

References

[1] T. Baba, I. Waki, Jpn. J. Appl. Phys. 35 (1996) L1134.
[2] M. Welling, H.A. Schuessler, R.I. Thompson, H. Walther, Int. J. Mass Spectrom. Ion Processes 172 (1998) 95.
[3] Y. Huang, G.Z. Li, S. Guan, A.G. Marshall, J. Am. Soc. Mass. Spectrom. 8 (1997) 962.
[4] C. Monroe, D.M. Meekhof, B.E. King, W.M. Itano, D.J. Wineland, Phys. Rev. Lett. 75 (1995) 4714.
[5] H.C. Nägerl, D. Leibfried, F. Schmidt-Kaler, J. Eschner, R. Blatt, Opt. Express 3 (1998) 89.
[6] H.A. Schuessler, E.C. Benck, J. Lassen, H.K. Carter, Hyperfine Interactions 81 (1993) 81.
[7] H.A. Schuessler, E.C. Benck, F. Buchinger, H.K. Carter, Nucl. Instrum. Methods Phys. Res. A 352 (1995) 583.
[8] M.G. Raizen, J.M. Gilligan, J.C. Bergquist, W.M. Itano, D.J. Wineland, Phys. Rev. A 45 (1992) 6493.
[9] H. Imajo, S. Urabe, K. Hayasaka, M. Watanabe, J. Mod. Opt. 39 (1992) 317.
[10] E.C. Beaty, J. Appl. Phys. 61 (1987) 2118. We use the values of set 6 in Table I.
[11] J.T. Höffges, H.W. Baldauf, W. Lange, H. Walther, J. Mod. Opt. 44 (1997) 1999.
[12] R.K. Melbourne, J.D. Prestage, L. Maleki, J. Appl. Phys. 69 (1991) 2768.
[13] M.A. van Eijkelenborg, K. Dholakia, M.E.M. Storkey, D.M. Segal, R.C. Thompson, Opt. Commun. 159 (1999) 169.
[14] K. Dholakia, G.Zs.K. Horvath, D.M. Segal, R.C. Thompson, J. Mod. Opt. 39 (1992) 2179.
[15] D.J. Bate, K. Dholakia, R.C. Thompson, D.C. Wilson, J. Mod. Opt. 39 (1992) 305.
[16] K. Hübner, H. Klein, Ch. Lichtenberg, G. Marx, G. Werth, Europhys. Lett. 37 (1997) 459.
[17] T.B. Mitchell, J.J. Bollinger, X.-P. Huang, W.M. Itano, Opt. Express 2 (1998) 314.
[18] W.M. Itano, L.R. Brewer, D.J. Larson, D.J. Wineland, Phys. Rev. A 38 (1988) 5698.